Short-duration accretion states of Polars as seen in *TESS* and ZTF data

C. Duffy [1,2]★ G. Ramsay [1] Kinwah Wu [3] Paul A. Mason,[4,5] P. Hakala,[6] D. Steeghs [2,7] and M. A. Wood[8]

[1]*Armagh Observatory and Planetarium, College Hill, Armagh BT61 9DB, UK*
[2]*Department of Physics, University of Warwick, Gibbet Hill Road, Coventry CV4 7AL, UK*
[3]*Mullard Space Science Laboratory, University College London, Holmbury St Mary, Surrey RH5 6NT, UK*
[4]*New Mexico State University, MSC 3DA, Las Cruces, NM 88003, USA*
[5]*Picture Rocks Observatory, 1025 S. Solano Dr. Suite D., Las Cruces, NM 88001, USA*
[6]*Finnish Centre for Astronomy with ESO (FINCA), University of Turku, Quantum, Turku FI-20014, Finland*
[7]*OzGrav: The ARC Centre of Excellence for Gravitational Wave Discovery, Clayton VIC 3800, Australia*
[8]*Department of Physics and Astronomy, Texas A&M University–Commerce, Commerce, TX 75428, USA*

ABSTRACT

Polars are highly magnetic cataclysmic variables which have been long observed to have both high and low brightness states. The duration of these states has been previously seen to vary from a number of days up to years. Despite this, these states and their physical origin have not been explained in a consistent manner. We present observations of the shortest duration states of a number of Polars observed by *ZTF* and *TESS*. This has allowed us to determine that short-duration states are a relatively common feature across the population of Polars. Furthermore, we have been able to generalize the model of star-spot migration to explain both short-lived high and low states in Polars by incorporating the interaction between the magnetic field of the white dwarf and that of the star spots.

Key words: accretion, accretion discs – binaries: close – stars: magnetic fields – novae, cataclysmic variables – starspots.

1 INTRODUCTION

Cataclysmic variables (CVs) are a class of close binary stars consisting of an accreting white dwarf (WD) primary and a late-type secondary, or donor, star. In these binaries, matter is transferred from the donor on to the WD via Roche lobe overflow through the L1 inner Lagrange point. In most cases the accretion flow takes the form of an accretion disc, as matter spirals towards the WD as a result of the viscosity of the disc. These systems often show distinct brightness states, known as high and low states, as a result of differing disc viscosity states and hence mass transfer rates e.g. the Z Cam-like binaries.

The formation of an accretion disc occurs if the WD in the CV is not strongly magnetic. If, on the other hand, the WD has a magnetic field that exceeds ∼10 MG, then an accretion disc may not form; instead, the matter accretes directly on to regions close to the WD magnetic poles – the plasma having been channelled by the magnetic field lines since passing through the L1 region. The strong magnetic interaction between the WD and its companion gives rise to a torque which forces the binary orbit, the spin of the WD, and the other components in the system into synchronous rotation. Such systems are known as Polars or AM Her systems after the archetypal source AM Herculis. See Warner (1995) for a review of CVs in general and Cropper (1990) and Wu (2000) for Polars and their magnetic-field channelled accretion in particular.

While about 140 Polars are now known, the mechanism(s) responsible for shutting off and on the mass transfer through L1 remain poorly understood. The Catalina Real-Time Transient Survey observed 44 Polars over a duration of 9 yr (Mason & Santana 2015). In that study, Polars identified to have short-lived low states included V1309 Ori, V834 Cen, and EQ Cet. Those undergoing short-lived high states included AR UMa, EF Eri, and HS Cam, while a few Polars – FL Cet, ST LMi, and BM CrB – have three brightness states. As they lack of an accretion disc, Polars are therefore excellent objects to study how the process of mass transfer can switch off and on in accreting binaries.

A second reason to study Polars is that they are ideal objects to study how accreting material in general interacts with strong magnetic fields. The magnetic field lines which the matter threads on to are determined by the ram pressure of the accretion flow. During a high rate of accretion the ram pressure is high and the material can penetrate deeper into the WD magnetic field than under a lower accretion rate. This allows the material to 'latch on to' different field lines and potentially accrete on to different or additional footpoints on the WD surface. Such changes in accretion geometry can be identified by changes to the orbital light curve of a system. In addition to the presence of different multiple or different accretion regions the observed emission from these regions can vary, it was proposed by Kuijpers & Pringle (1982) that accretion can proceed via a method termed 'blobby accretion'. Under this model individual 'blobs' of material accrete along the magnetic field lines as opposed to a continuous stream. This model has been successful in explaining differences in accretion at different poles (Hameury & King 1988; Schwope et al. 2020).

★ E-mail: christopher–duffy@armagh.ac.uk

In addition to Polars, state transitions have been observed in Intermediate Polars (IPs) and VY Scl stars. Unlike Polars these types of CVs have accretion discs to some degree and while this brings additional considerations to the mass transfer properties, it offers us an additional population of objects to aid us gain insight into state transitions in Polars. IPs are magnetic CVs with a magnetic field <10 MG, as such unlike their more strongly magnetic cousins they do form a (truncated) accretion disc. Recently, Covington et al. (2022) investigated the low states in IPs. Of the systems which they investigated all but one exhibited long-lived (of order months and years) low states. This implies that IPs are predisposed to more long-lasting and stable state changes than those often seen in Polars. Some IPs are thought to be, at least at times, disc-less, and at least in the case of YY Dra (DO Dra) can have short-lived low states (Hill et al. 2022). This suggests that mechanisms behind low state formation in stream accreting IPs are different than for the usual IPs with discs. For example, the disc may have a screening effect for the WD magnetic field at L1 as well as acting as a buffer between changes in mass transfer through L1 and the observed accretion rate on to the WD.

The archetype Polar, AM Her, displays frequent state transitions and as such has been the subject of most of the investigations into state transitions in Polars, and hence is a useful object to consider at length. AM Her was the first Polar to be identified, because of its brightness (high state brightness ∼13.5 mag), and its strongly polarized optical radiation was discovered to vary with the binary orbital period of 185.6 min (Tapia 1977). AM Her has been studied at length, with optical data going back over 100 yr. As such, the long-term macro behaviour of AM Her has been extensively studied (e.g. Ramsay, Cropper & Mason 1995; Wu & Kiss 2008; Šimon 2016). In particular, AM Her is known to exhibit two different brightness states: a high and low state. As opposed to many other CVs, which have different brightness states which they transition between with a singularly defined recurrence time and duration of states, AM Her shows a mixture of long and short, low and high, states which can last from several days to months for low states, and several months to years in the case of high states, with as-yet no discernible overall pattern. Consequently, it has been a challenge to quantify the long-term behaviour of AM Her. Efforts to this end have identified that there are a number of different timescales upon which these different states occur and have verified that these timescales and state duty cycles can be determined, however their presence is intermittent (Wu & Kiss 2008; Šimon 2016).

Wickramasinghe et al. (1991) found that during the high state of AM Her, the material accreted on to two distinct regions on the WD: a primary and a secondary. The primary region is believed to occupy part of the face opposite the donor and accounts for the majority of the mass transfer and emission (see fig. 18 of Wickramasinghe et al. 1991). The secondary accretion region is found on the donor star facing surface of the WD, however at a separation substantially less that $180°$ from the primary. This fact excludes the simplest models for explaining the behaviour seen in AM Her, namely that of centred dipole (Wu & Wickramasinghe 1993). This has been reinforced by observations of other Polars which indicate that the primary accretion region has a magnetic field ∼2 orders of magnitude weaker than that found at the secondary region (Ferrario et al. 1989; Wickramasinghe, Ferrario & Bailey 1989; Schwope, Beuermann & Thomas 1990). Wickramasinghe & Wu (1991) presented a multipole model comprising of a dipole and quardupole in the WD and an intrinsic dipole in the donor star and further elaborated it in Wu & Wickramasinghe (1993) to explain the observations of accretion geometry and distribution of magnetic field strengths between the accretion regions. While the model provided an explanation to the

general accretion behaviour of Polars, and AM Her in particular, the precise location of the accretion region remains a subject for more thorough investigations. Efforts to map the cyclotron emission region have some gained success in a number of systems, e.g. CD Ind (Hakala et al. 2019).

In the low state, with reduced mass transfer, AM Her was observed to accrete on to only one pole. Wu & Kiss (2008) suggested that this transition into a low state was due to a realignment of the system magnetic field with the WD being the key component regulating mass transfer. This is an extension of an earlier proposition by Livio & Pringle (1994), in which the suppression of the mass transfer that leads to the low state is caused mainly by the migration of a star-spot or several star spots on the donor star to regions close to the L1 point of the binary. While promising, this scenario needs further development so as to provide a self-consistent explanation for the duration and frequency of the low states observed in some systems. More specifically, it must explain how the secondary stars, which are low-mass M stars, generate a sufficient quantity of star spots and what mechanisms entice the star spots to migrate to regions sufficiently close to the L1 point such that the mass transfer would be efficiently disrupted (see e.g. Hessman, Gänsicke & Mattei 2000). Nonetheless, the study of Kafka & Honeycutt (2005) identified that the timescale of the transition into a low state in AM Her, and other Polar above the period gap, was consistent with that expected of the star-spot scenario.

In this work, we seek to further understand the mechanism which controls these state changes and explain both the short-duration high and low states in a consistent fashion. To that end we present observations of a number of short-duration states in Polars in both the *Zwicky Transient Facility* (*ZTF*) and the *Transiting Exoplanet Survey Satellite* (*TESS*). We use these observations to probe the properties of these state changes and to develop an understanding of the changes in accretion geometry which are associated with them.

2 PHOTOMETRIC DATA

In looking for short-duration state changes among Polars we focused on two different data sets: *ZTF* and *TESS*. *ZTF* is a time domain survey program using the Palomar 1.2m telescope; covering 47 deg^2 per exposure ZTF is able to survey large areas of the sky rapidly building up light curves of diversely located sources to a limiting brightness of ∼20 mag. Observations are made in three different filters, ZTF-*i*, ZTF-*g*, ZTF-*r*, although in this work we limit our analysis to the *g* and *r* bands (∼4087–5522 Å and ∼5600–7316 Å, respectively) as the observing program employed by *ZTF* results in these filters having the highest cadence (see Bellm et al. 2019, for a full description).

TESS is a space-based optical observatory launched in 2018. It has an observing strategy of making CCD observations with four wide-field telescopes, each with a $24° \times 24°$ field of view. The observing plan splits the sky into 26 set sectors spanning from the ecliptic to the ecliptic poles. Each of these sectors are observed continuously for approximately 27 d with a short gap at the mid-point for data transmission and momentum unloading. During an observation, 120 s cadence photometry is generated on a series of predefined targets (see Ricker et al. 2015, for full *TESS* details).[1]

---

[1]The sources in this paper were included on the 2 min cadence list due to their inclusion on the following Guest Investigator programs: GO11256/PI Garnavich; G011268/PI Scaringi; G022071/PI Scaringi; GO22116/PI
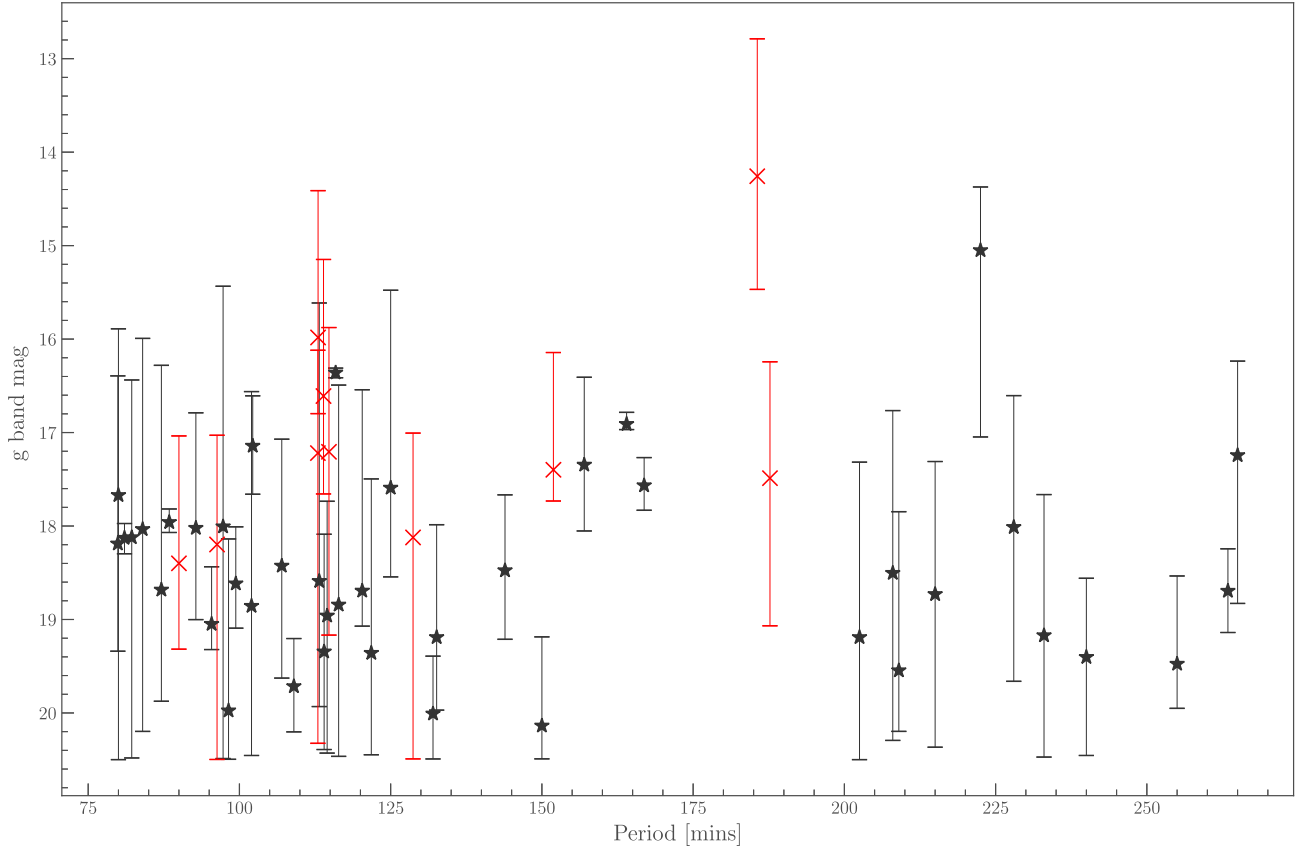
Figure 1. Period distribution of the Polars contained within the ZTF sample considered as the mean *g*-band magnitude as a function of period. The error bars show the max–min range of the brightness. The entries which are shown in grey with a ⋆ denote those systems which do not show short transitions; the entries shown in red with an X denote those which do show transitions. Full listing of these sources is contained in Table B1.

2.1 ZTF data

We accessed photometric data of 60 known Polars (Ramsay, private communication) collected by *ZTF* (see Table B1 for full details). Of these, 55 sources were deemed to have enough data for analysis, i.e. at least 25 data points in both ZTF-*g* and ZTF-*r*. The distribution of this sample is illustrated in Fig. 1 which shows the mean *g*-band magnitude of the sources as a function of their period, with error bars used to denote the magnitude range of the system. This distribution clearly shows the period gap, below which the majority of Polars are found. We see that systems below the period gap show a greater spread in magnitude range with systems that vary by as little as ∼0.2 mag to as much as ∼4 mag, whereas those systems above the period gap have a more consistent magnitude spread of ∼2.4 mag.

These sources were first visually inspected for brightness state changes. For those systems exhibiting a state change, we performed subsequent analysis. This inspection revealed that within the state changing systems there were three categories of behaviour: systems which showed 'long' lived state changes, systems which showed 'short' lived state changes, and systems which showed both. Examples of systems which show each such behaviour are shown in Fig. 2, which also shows an example of 'short' lived

state changes where brightness increases as well as those where it decreases; the full listing of behaviours can be found in Table B1.

We established a definition of 'short' lived state changes to be those which had a duration, the time between onset and the return on the original brightness, of ≲60 d. This was established via a combination of inspection of the population of light curves and comparison with previous studies by Kafka & Honeycutt (2005).

We employed two methods to establish the duration of states depending on density and temporal distribution of the data available. Whenever the data sampled the short-duration state and its transition sufficiently well, we undertook a non-linear curve fitting approach. Using the Python module lmfit (Newville et al. 2021), we defined the short-lived state as a composite of a skewed Voigt profile to fit the short-duration state, and as a constant function to fit to the proceeding and succeeding state. As a convolution of the Gaussian and Lorentz profiles the Voigt profile comprises of two parameters which control the width of the curve: σ and γ. In initial tests using this model we set these parameters to be independent but we found that they both converged on the same value, as such the analysis was carried out under the assumption that they were of equal value.

We performed our minimizations using a Markov chain Monte Carlo (MCMC) algorithm using the emcee (Foreman-Mackey et al. 2013) Python module to do so. Although this increased the analysis compute time compared to a least squares minimization, it improved the robustness of our fits by allowing us to visualize the parameter space and to minimize and isolate uncertainty in individual fitted parameters in order to improve our confidence in a given fit.
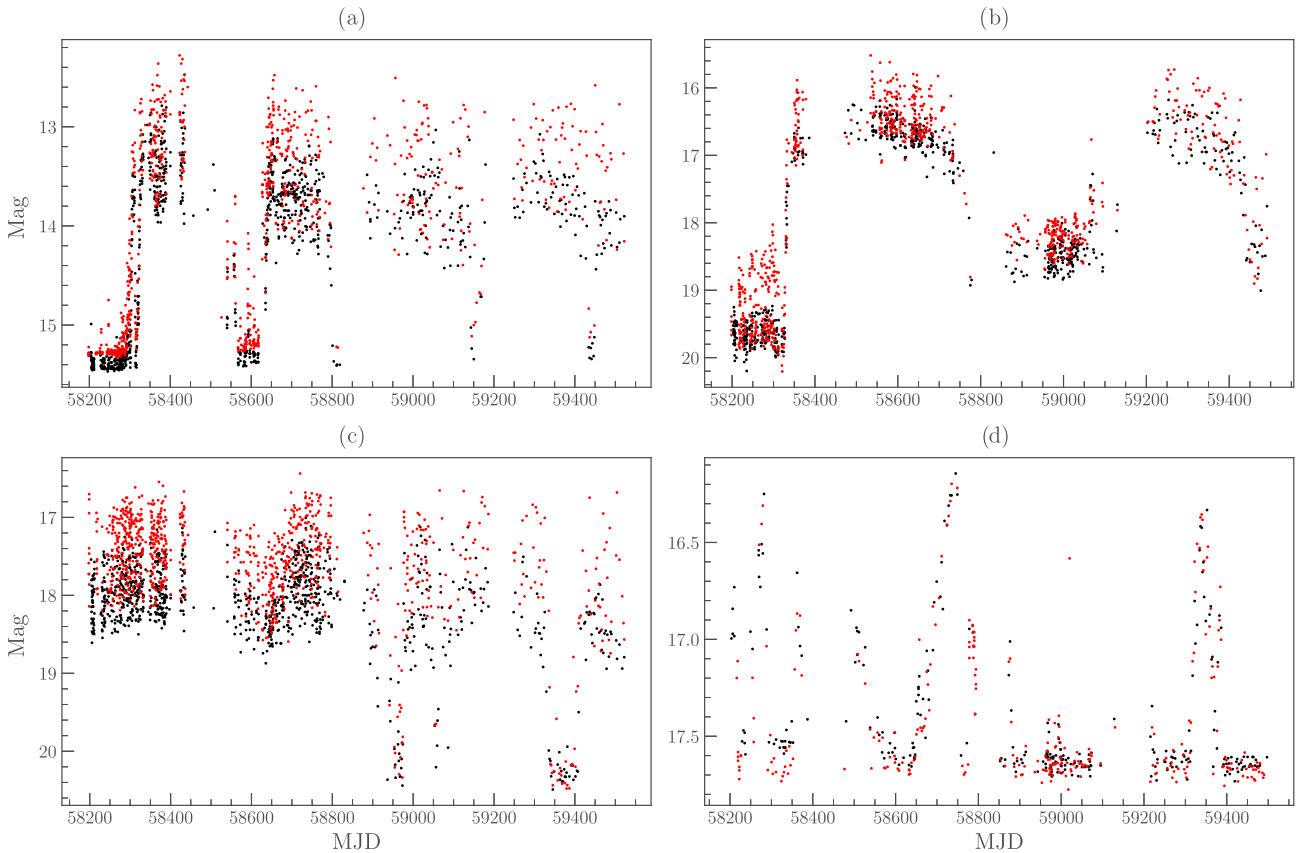
Figure 2. Light curves of four of the objects considered with *ZTF* data coloured red and black to denote ZTF-*r* and ZTF-*g*, respectively, showing (a) AM Her with both long- and short-duration states, (b) SDSSJ154104+360252 which shows only long-duration state changes, (c) MT Dra which shows only short-duration state changes, and (d) AP CrB which shows only short-duration state changes to a higher state.

We established the duration of the fitted short-lived states from the full width at half-maximum (FWHM) (or minimum) value for the Voigt profile. In a Voigt profile this is approximated in a relationship with the FWHM values, F, of the Gaussian component, equation (1), and the Lorentzian, equation (2):

$$F_G = 2\sigma \sqrt{2\ln(2)} \tag{1}$$

$$F_L = 2\gamma, \tag{2}$$

with $\gamma \equiv \sigma$. These are combined to give the following approximation of the FWHM of the Voigt profile which is accurate to $\sim \pm 0.02$ per cent (Olivero 1977):

$$F_V \approx 3.60\sigma. \tag{3}$$

Fig. 3 shows the 1D marginalized posteriors of the value of sigma extracted from the results of the MCMC calculation on the fit of a state transition seen in MT Dra, which is shown in the lower panel. This indicates the quality of the fit, particularly with respect to the parameter key to the duration determination; furthermore, it illustrates the applicability of the model used to fit these transitions.

The calculated duration of all of these states is contained within Table 1. When more than one short-lived state was observed, the mean duration value is shown. In those cases where the data did not permit us to undertake a curve fitting approach, we undertook a visual inspection. This does not allow for the same level of precision available in cases where model fitting is possible, but it ensures that sources which do show these features are not neglected. By
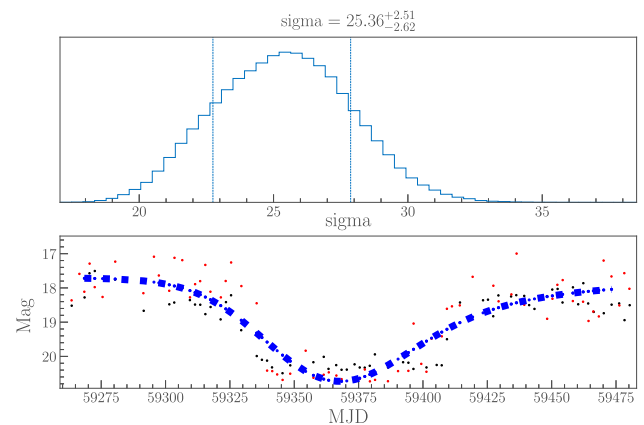

Figure 3. Upper panel: the result of the marginalization of the sigma parameter, extracted from the multiparameter analysis for a state transition in MT Dra. Lower panel: the fitted state transition in MT Dra and the fitted data. The red data points indicate *r*-band data and the black data points indicate *g*-band data.

combining these methods, the systems which were found to meet these criteria are listed in Table 1 and highlighted in Fig. 1 where they are marked with an X and coloured red.

In Table 1, four sources have ancillary values quoted in brackets for some of their parameters. In the case of ST LMi, five short-lived states are observed; however, we were only able to resolve three in

Table 1. *ZTF* sources which show short-lived state changes. The table shows the number of events, their mean duration, and mean recurrence. The mean durations marked with † are derived partially from visual inspection and †† denotes mean durations derived entirely from visual inspection. The values contained within brackets are ancillary values calculated on the basis explained in Section 2.1. Errors arise from fit confidence values or the standard deviation where visual inspection was used. Full details of sources can be found in Table B1.

Source	g_{mean}	States	Duration [d]	Recurrence [d]
FL Cet	19.15	4	$40.9^{\dagger\dagger} \pm 10.7$	180 ± 158
AN UMa	17.21	1	$53.1^{+5.8}_{-4.8}$	–
RXJ1610+03	17.49	1	$40.1^{\dagger\dagger}$	–
EU UMa	18.40	1	$39.9^{+3.7}_{-3.9}$	–
ST LMi	16.61	3 (5)	$24.1^{\dagger\dagger} \pm 7.6$	273 ± 90
MT Dra	18.12	2 (3)	$27.5^{\dagger} \pm 8.9 \ (49.5)$	110 (196)
AM Her	14.26	2 (4)	$21.7^{\dagger} \pm 7.3 \ (27.6)$	297 (288)
AP CrB	17.40	4 (5)	$33.9^{\dagger} \pm 15.6 \ (42.7)$	$368 \pm 201(276)$
V2301 Oph	17.22	1	$37.4^{+5.7}_{-4.1}$	–
BS Tri	18.20	1	$19.1^{\dagger\dagger}$	–
V884 Her	15.98	3	$49.6^{\dagger} \pm 6.1$	389 ± 40

order to calculate the duration. Despite this, all five were used to calculate the mean recurrence time. In each MT Dra and AP CrB, we observed an additional short state which took the same profile as the others seen in the respective light curves but had a duration longer than our definition for a short-duration event (69.1 and 93.4 d). For these sources, the values contained within brackets relate to the inclusion of these events. Finally, in AM Her we observed two events within quick succession, ∼2 d; individually these events would fit in our criteria; however, if they are in actual fact a single event then it would not and we cannot with absolute certainty say that these are separate events. As such, we have included these two events and their related parameters as ancillary values.

We identified 11 sources which show short-lived state changes. This accounts for 18.3 % of the original sample considered. Of the systems identified it can be seen clearly in Fig. 1 that they disproportionately, albeit not exclusively, lie below the period gap. Within this distribution there is a particular bunching of four sources with periods of ∼113 min. Overall, the mean duration of short-lived state transitions observed was 35.2 d, increasing to 38.5 d if ancillary values in the three cases discussed above are included. Similarly, the mean recurrence time of those systems which show multiple events is 270 d falling only slightly to 267 d when the ancillary values are included. No discernible relationship appears to exist connecting recurrence time or duration to either the orbital period or the *B* field strength. We furthermore performed an Anderson–Darling test on the period distributions of the sources with and without short-duration states; this yielded no evidence of a significant difference in the distribution of each population.

2.2 *TESS*

We accessed *TESS* 2 min photometry on nine Polars through the Python module `lightkurve` (Lightkurve Collaboration 2018). The high temporal resolution offered by *TESS* allowed us to both study the short-lived states in more detail, which had been identified in the ZTF data and probe sources for short-duration events that could not otherwise be resolved. Table 2 summarizes the sources studied and identifies those in which a short state occurred.

The events which we identified fall into three broad categories: short-lived dimming and brightening events, both of which have

a duration ≲5 d, and the third category is the counterparts of the events which had previously been identified from the ZTF data. Fig. 4 show examples of each of these, where the *TESS* light curve is shown in black with the same binned upon the known orbital period superimposed in red. In total, we identified five sources with one of these behaviours. Using these findings from *TESS* we are able to observe how the orbital light curve of these sources change as a result of moving into and out of these states (Section 2.3). We can then use this to infer how, if at all, the accretion geometry has changed as a result of the state change, which could help us determine how the accretion flow attaches on to different magnetic field lines depending on the mass transfer rate or other factors.

Although the number of systems identified in *TESS* data to show short-duration outbursts is small and cannot be used to draw population-wide conclusions, we note that those systems with the shortest events visible only in *TESS* appear to be biased towards longer period systems. However, as we identified no relationship connecting state duration to the orbital period, we consider that this is most likely simply the result of small number statistics.

2.3 Orbital profile light curves

In each of the sources in Table 2 for which we found to contain short-lived state changes, we used the *TESS* data to investigate how the light curve phased upon the orbital period (henceforth the orbital light curve) evolved as the sources moved between their states. In each case we extracted a portion of the *TESS* light curve which corresponded to the short-duration state which we subsequently folded upon the known orbital period and then binned. This process was then repeated with other segments of similar duration from the light curve outwith the short-lived state. This allowed us to compare the orbital light curves in various states and to identify any differences; in this manner it is possible to constrain the accretion geometry of each state and to understand how it evolves.

Typically, in Polars accretion is generally described as being either one or two pole. In one-pole accretion the accretion region is behind the WD not always visible to us, whereas in two-pole systems the orientation of the system is such that one of the accretion region is always visible as the system rotates. Each of these scenarios creates a different orbital light-curve signature (Cropper 1990). As the mass transfer rate in a system changes, the ram pressure of the flow changes accordingly, so material can become captured by different sets of field lines which can result in matter accreting on to different regions of the WD. As such, this can result in a change in the observed orbital light curve and provides insight towards the underlying accretion geometry.

2.3.1 QQ Vul

In Fig. 5, we show the folded and binned orbital light curve of QQ Vul before, during, and after the short-duration reduction in brightness. The orbital light curves before and after the dip are unsurprisingly similar, indicating that the initial accretion state is re-established after the dip. The high state orbital light curve is similar to the 'Type 1' state identified by Kafka & Honeycutt (2003), where there is only an optical signature from 1 pole. Conversely, the light curve during the dip is similar to the 'Type 2' state, which shows an optical signature from a second pole. This dip event lasts for ∼2 d, which is slightly shorter than the finding of Kafka & Honeycutt (2003) who note they usually persists for more than 3 d.

Cropper (1998), Schwope et al. (2000), and Kafka & Honeycutt (2003) indicated that QQ Vul may be a two-pole accretor. X-ray

Table 2. Properties of the *TESS* sources considered and the sectors in which they were observed by *TESS*. The quoted magnitudes are sourced from *Gaia* eDR3.

Source	Sectors	Mean G mag	Period [min]	Inclination	Transition	Notes
BL Hyi	1, 2, 29	19.1	123.6[a]	32°[b]		
CW Hyi	1, 2, 27–29	17.5	181.8[c]	45°–85°[d]	✓	2–3d reductions in brightness
FL Cet	4, 42, 43	18.6	87[e]	–		
MR Ser	24, 25	16.1	112.3[f]	45°[g]		
MT Dra	14–16, 18–26, 40, 41	17.5	128.7[h]	≤70°[h]	✓	Contemporaneous observations of ZTF state
UW Pic	5, 6, 31–33	15.9	132.5[i]	45°–75°[i]		
AM Her	14, 25, 26, 40, 41	14.3	185.6[j]	35°–60°[k]	✓	Contemporaneous observations of ZTF state
V834 Cen	38	16.6	101.5[l]	45°–60°[m]	✓	∼4d increase in brightness
QQ Vul	41	15.3	222.5[n]	∼50°[o]	✓	∼2d reduction in brightness

Notes. Citations: [a]Agrawal, Riegler & Rao (1983), [b]Beuermann et al. (2007), [c]Schwope et al. (2002), [d]Burwitz et al. (1997), [e]Szkody et al. (2002), [f]Schwope et al. (1991), [g]Brainerd & Lamb (1985), [h]Schwarz et al. (2002), [i]Romero-Colmenero et al. (2003), [j]Kafka et al. (2005), [k]Schwope et al. (2020), [l]Mason et al. (1983), [m]Schwope et al. (1993), [n]Nousek et al. (1984), [o]Cropper (1998).
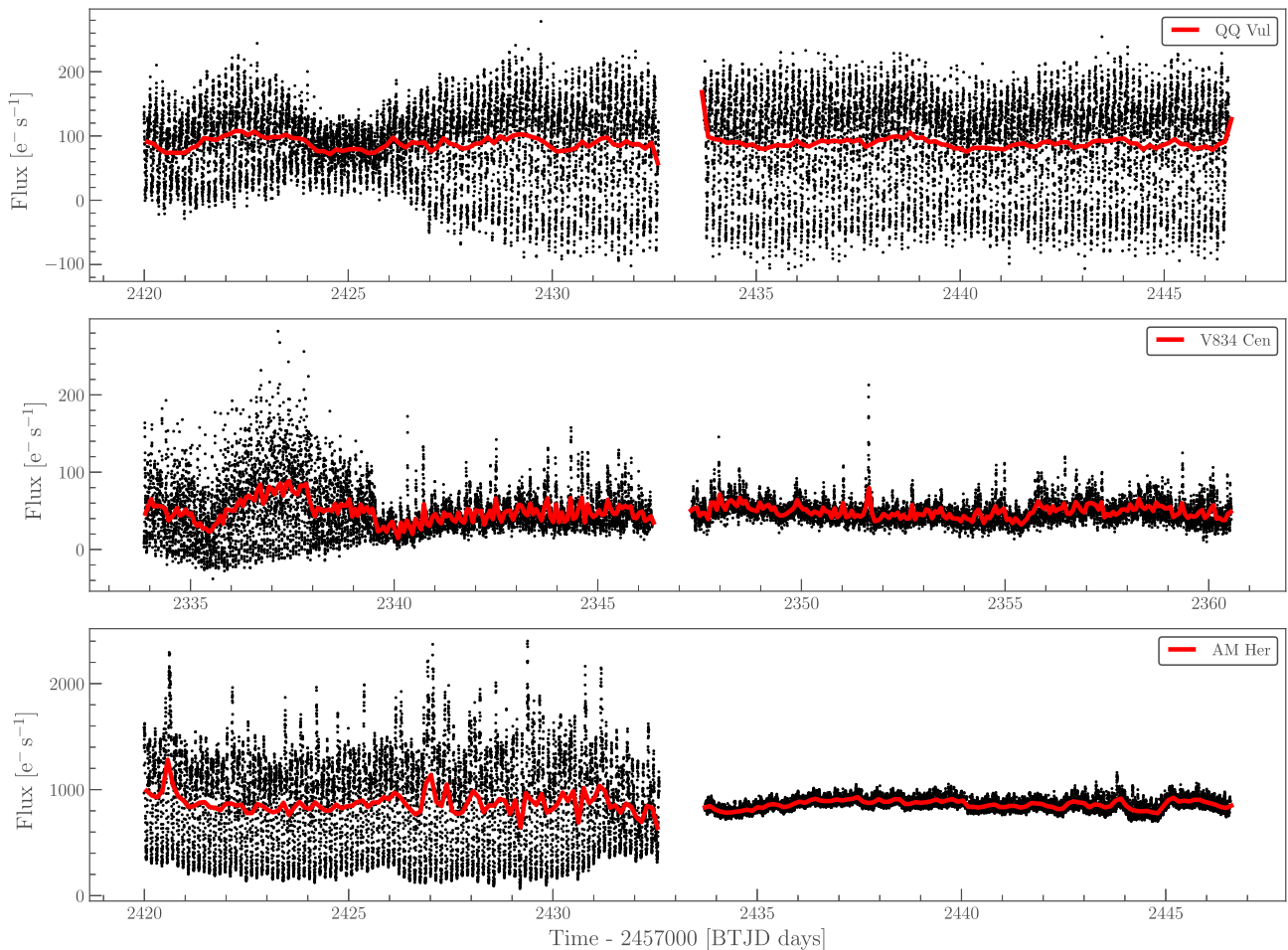
Figure 4. *TESS* light curve of (a) QQ Vul sector 41, (b) V834 Cen sector 38, and (c) AM Her sector 41. In each panel, the light curve binned on the known orbital period of the source is shown in red.

observations made by Belle, Howell & Mills (2000), which coincided with a 'Type 1' state, optical observations were shown to originate from two-pole accretion. This indicates that this configuration has two-pole accretion but that the second pole does not leave an optical signature. While the mean brightness during the dip understandably decreases, the orbital minimum at this time is actually brighter. This suggests that a new accretion footpoint is established at this time.

2.3.2 V834 Cen

In Fig. 6, we present the folded and binned orbital light curve of V834 Cen during the short enhanced brightness event which occurs at the start of the sector 38 observations and the profile immediately after this event. Unlike QQ Vul, the two light curves shown here are essentially identical, notwithstanding the scale of
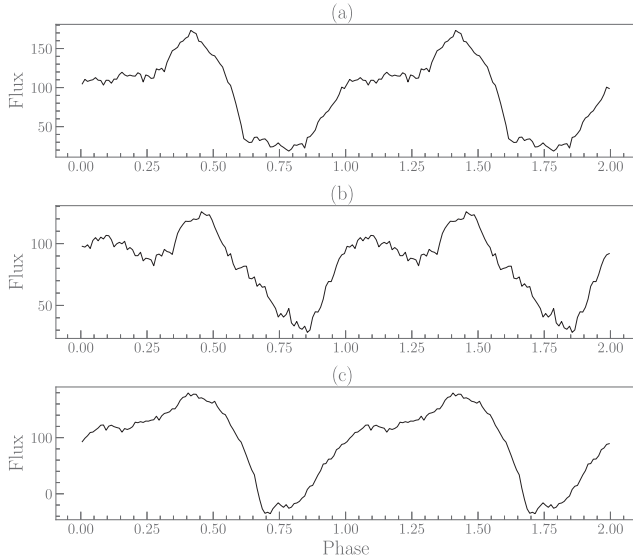
Figure 5. Folded and binned light curve of QQ Vul (a) before the decreased brightness event (BTJD = 2420-2423.5), (b) during decreased brightness event (BTJD = 2423.5-2426.5), and (c) after the decreased brightness event (BTJD = 2426.5-2430.5). All three have been phased with an epoch set to the start of sector 41.
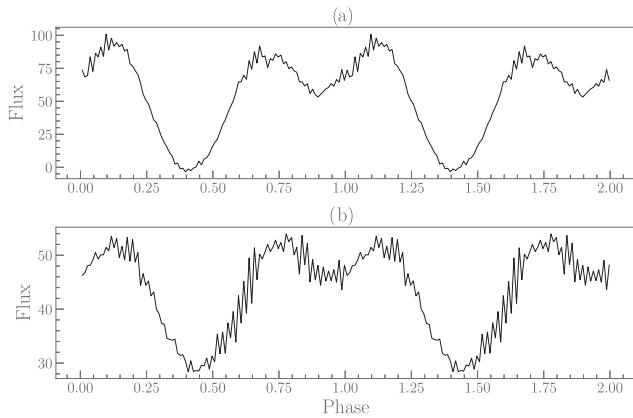

Figure 6. Folded and binned light curve of V834 Cen (a) during the increased brightness event (BTJD = 2334-2339.6) and (b) after the increased brightness event (BTJD = 2339.6-2346.3). Both have been phased with an epoch set to the start of sector 38.

the brightness changes. This implies that the accretion geometry remains unchanged, and that matter accretes along the same field lines in both. The orbital light curve presented here is consistent with the earlier findings of Cropper, Menzies & Tapia (1986, cf. fig. 8). That work also presents a different orbital light curve (cf. fig. 9) which is suggested as part of the evidence that the accretion stream's location is not fixed. As we do not see this difference between the brightening event and the subsequent dimmer state, we are confident that the accretion stream has a fixed location between these two states.

In the state which follows the event, we see between phases 0.50 and 0.70 an increase in the root-mean-squared deviation of the orbital light curve. Comparing with the unfolded light curve in the middle panel of Fig. 4, we see that this is associated with repeated flare-like events that occur during this state. These events reoccur at approximately the same phase causing them to appear as they do
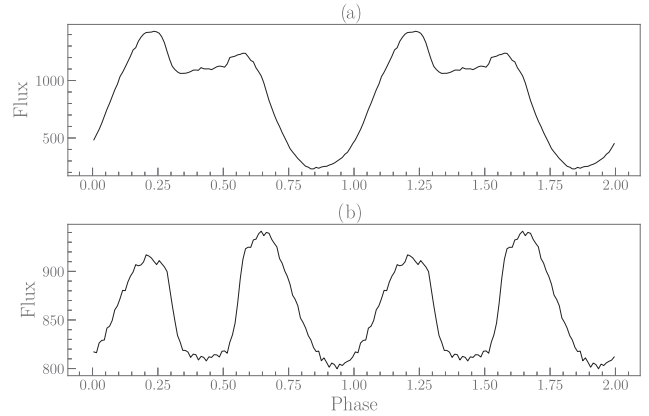

Figure 7. Folded and binned light curve of AM Her (a) during the initial high state (BTJD = 2420-2432.6) and (b) during the short low state (BTJD = 2433.6-2446.6). Both have been phased with an epoch set to the start of sector 41.

on orbital light curve. Similar events have been seen by Middleditch et al. (1991) and Mouchet et al. (2017) occurring at the same orbital phase. The origin of these events has not yet been determined. However, these 'flares' disappear during the enhanced accretion event, which may be associated with the colour dependency of the flares at different mass transfer rates as identified by Middleditch et al. (1991); however, given the broad bandpass in *TESS* this seems unlikely. A more plausible explanation is that the accretion we are seeing at this time is dominated by 'blobby' accretion, and as each blob of material accretes we see an associated increase in brightness.

2.3.3 AM Her

In Fig. 7, we show the folded and binned orbital light curve of the high state in AM Her and the short-duration low state which immediately followed, both of which were seen in sector 41. The low state has a distinctly different orbital light curve from that seen in the high state with two clear stand-alone peaks. Although the peaks in the low state occur at approximately, but not exactly, the same phase as in the high state, albeit at much lower flux values, the relative strength of these peaks are reversed as the first peak shows a greater reduction in flux than the second.

The orbital light curve during the high state which we have presented here is consistent with that found by Gänsicke et al. (2001) when observing the high state of AM Her in the *V* band. They identified this light curve to be dominated by cyclotron emission from the main accretion pole. Kafka et al. (2005) performed a multiwavelength study of AM Her in a low state, and in particular obtained photometry in *JHK* bands. The *TESS* low-state observations here match the *J*- and *H*-band observations, whereas the *K*-band light curve was more reminiscent of the high state. Their findings confirmed that accretion via Roche lobe overflow had effectively ceased, but that the profile was dominated by cyclotron emission even in this low mass-transfer state. Our findings are entirely consistent with these observations.

2.3.4 CW Hyi

In Fig. 8, we show the orbital light curves of CW Hyi before, during, and after the short reductions in brightness seen in sectors 27 and 28. We found that folding the light curve upon the 181.8 min period reported by Schwope et al. (2002) resulted in a phase drift of 0.3
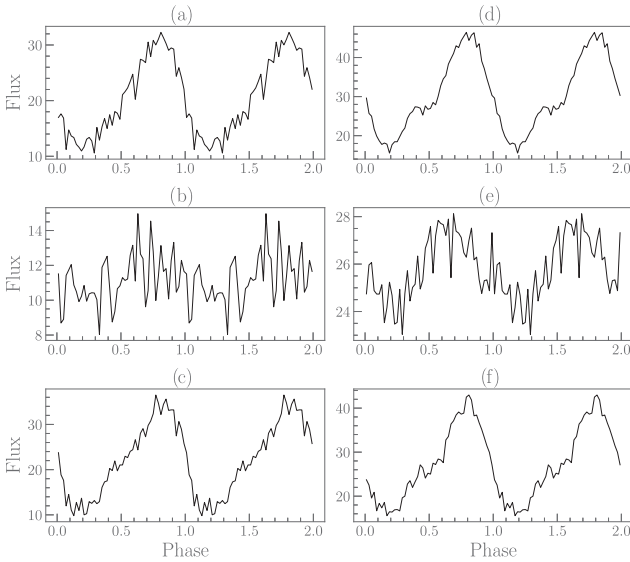
Figure 8. Folded and binned light curve of CW Hyi (a) before the sector 27 dimming Event (BTJD = 2053.8-2054.9), (b) during the short-duration low-state Event (BTJD = 2054.9-2055.9), (c) after the Event (BTJD = 2055.9-2056.9), (d) before the sector 28 dimming Event (BTJD = 2066.5-2068.5), (e) during the short-duration low-state Event (BTJD = 2068.5-2070.5), and (f) after the event (BTJD = 2070.5-2072.5). All of the profiles have been phased with an epoch set to the start of sector 27.

Figure 9. Folded and binned light curve of MT Dra (a) the high state seen during sector 26 (BTJD = 2023.1-2035.1) (b) during the Event (BTJD = 2390.6-2404.4), (c) after the Event (BTJD = 2407.5-2418.9). All three have been phased with an epoch set to the start of sector 40.

cycles per *TESS* sector. Investigation of the *TESS* data revealed an orbital period of 181.55 min. This improvement in the period eliminated the phase drift and thus we have used it for the remainder of our analysis.

The orbital light curves before and after each event are very similar; this is in contrast to the light curves of the two lower states which show differences. Though it is possible to identify the original shape of the orbital light curve in the sector 27 event, it is substantially diminished such that we believe that this marks a ∼1.5 d cessation in accretion. The event in sector 28 on the other hand does not have the same brightness reduction, which is likely why the shape can be more easily recovered. In this event, we do not believe that accretion has ceased; it has only reduced while retaining a similar accretion geometry. We were able to access limited contemporaneous All Sky photometry via AAVSO[2] which indicated that outwith the events seen CW Hyi was in the same brightness state as it is usually found (mag ≃ 16.5–18.5). This supports our contention that these are very short-duration, possibly unstable, low states where accretion is dramatically reduced or stopped entirely.

Comparing those orbital light curves outwith both of the events discussed here with those presented by Schwope et al. (2002) and Cieslinski et al. (2010) shows good agreement in both shape and brightness variation. Schwope et al. identified this single-peaked feature to be the signature of single-pole accretion with the flux originating from beamed cyclotron emission. No published work presents orbital light curves of CW Hyi which appear similar to those of the dimming event nor have such events been reported before; consequently, we believe that this is the first time a state transition of any sort has been identified in CW Hyi.
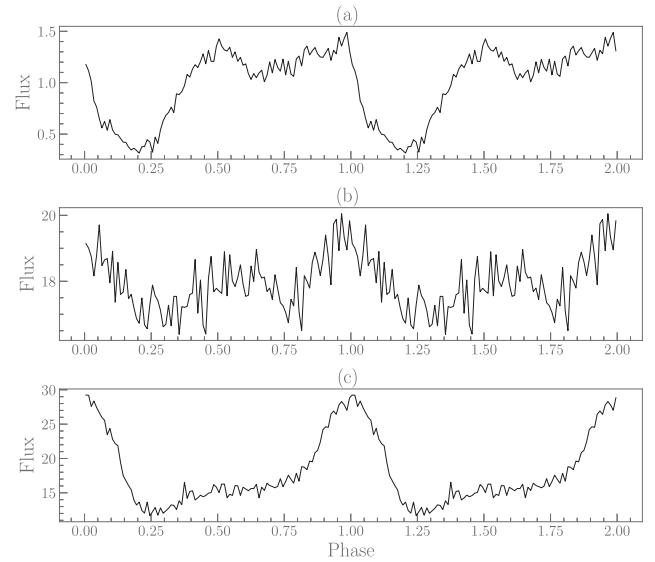
---

[2]The American Association of Variable Star Observers: aavso.org

2.3.5 MT Dra

In Fig. 9, we present the folded and binned light curves of MT Dra before, during, and immediately after the low state centred on MJD = 59347 (see Fig. 2c). The orbital light curve before and during the event both show two peaks, suggesting that two-pole accretion is taking place, albeit at markedly different rates. However, without polarimetry it is not possible to confirm this, as it is possible that cyclotron beaming has produced two maxima from emission of from a single pole. As both peaks appear at the same phase, we believe that matter is accreting along the same field lines on to the same regions in each case. The single-peaked nature of the state after the event suggests that this state is one of the single-pole accretion with matter accreting along one of the footpoints of field lines seen in the two-pole case.

Our findings differ from Zubareva et al. (2011) who identified a single-peaked light curve in the low state and a double-peaked light curve in the high state. Furthermore, while the scale of the brightness variation across the orbital period in both high states is consistent with these earlier findings, the scale of the brightness variations in the low state is markedly reduced from $F_1/F_2 \simeq 5.7$ in that work to $F_1/F_2 \simeq 0.1$. Zubareva et al. report evidence for an extended low state lasting longer than reported here, additionally being >1 mag brighter compared to Fig. 2 (c) though the brightness of both high states are consistent. This implies that we have identified an even lower 'low' state in MT Dra where accretion occurs on to two poles.

It is not clear why the high state which immediately follows the low state has a different profile. Although there maybe several reasons for this, we note that the flow through L1 is affected by magnetohydrodynamic (MHD) conditions at L1. The local magnetic field configuration depends on the combination of local spot fields, the global donor field, and the WD magnetic field. For the light curve to return to the same shape, the local field configuration must also return to a comparable state as it directly affects mass transfer through the L1 region.

3 DISCUSSION

Low states in Polars are a natural consequence of a substantial decrease in the mass transfer rate or a temporary disruption of the mass-transfer process. While the former can be caused by the secular evolution of the binary, both the former and the latter can be caused by an alternation in the MHD properties of the companion star near the L1 point. A possible cause of the suppression of mass outflow from the companion star is the adjustment of the topology of the magnetic field at the L1 region, which may be a response to the change in the magnetic configuration set by the WD and the companion star (see Wu & Kiss 2008). Another possibility is the magnetic field near the L1 point is readjusted in response to the migrating in of a large star-spot or a cluster of star spots (see Livio & Pringle 1994; Šimon 2016). The essence of these scenarii is that the magnetic field configuration at the L1 region is modified. It does not require an atmospheric response of the whole companion star that would in turn invoke more complex mechanisms, such as irradiation by the accreting WD, which leads to a building up period for the mass-transfer and irradiation feedback (see e.g. Wu, Wickramasinghe & Warner 1995). This scenario in the framework of magnetic star spots is therefore more appealing and is of particular relevance in the context of the transitions into low states which we present here.

VY Scl stars are a subclass of nova-like (NL) CVs which exhibit pronounced low states; they are a relatively rare subclass within the NL CVs with Honeycutt & Kafka (2004) noting that from a sample of 65 NLs only $\sim 15\%$ of them exhibited the phenomenon and of that sample only a single system exhibited a state change of similar duration to those presented here. Unlike Polars however, VY Scl systems have accretion discs and lie almost exclusively above the period gap. It is thought that VY Scl stars move between the two stable configurations for disc accretion offered by the disc accretion model: a hot large disc for the high state and a small cool disc for the low state (Warner 1995). The long running challenge with these systems has been to explain why they do not show outbursts during the transition between states, with competing models suggesting a truncated disc caused by irradiation of the inner disc (Leach et al. 1999) or considering that the WD is magnetic and that VW Scl stars are in actual fact IPs (Hameury & Lasota 2002). Despite lacking a comprehensive understanding of the states in these systems, it is still instructive to compare the low states with those we have explored here.

It is clear that although similarities exist between low states in Polars and those seen in other types of CVs, there are a number of significant differences. The observations which we present here indicate that Polars are capable of short-duration low states and exist in a number of systems such as to make it a not so uncommon occurrence, whereas in IPs and VY Scl systems this is uncommon.

In the following discussion, we will explore the short-duration low and high states and their possible physical origins and how these vary, or otherwise, with the states seen in over systems. Furthermore, we explore the changes in the orbital light curves as a result in these changing brightness states and how that informs the accretion geometry of these systems.

3.1 Short-lived low states

Out of those systems which we identify as containing a short-lived state change the most common manifestation of this was a low state. In 11 cases, nine in the *ZTF* sample and two in the *TESS* sample, we observed multiple events pointing to the origin of these short-duration states being a feature that is relatively common within Polars that

can form with ease as opposed to requiring rigorous or difficult-to-establish conditions. Despite having determined recurrence times for a number of systems, we found no correlation between this and either *B*-field strength of the WD or orbital period; similarly, no such relation could be robustly developed with respect to the duration of these states. This notwithstanding, however, we do note that the shortest duration events seen only in *TESS* appear to originate in systems with longer periods, though the small number of systems that showed these shortest duration states mean that this may be a statistical quirk. Additionally, though no obvious correlations with orbital period appear to exist, we do note that the systems which we see to posses short-lived state changes appear to be predisposed to lie below the period gap at a rate greater than the overall population of Polars.

The duration of these short-lived low states appears to be variable within our definition of short-lived; between a few days up to ~ 50 d. The duration of these low-states and their common occurrence essentially rules out that low-states are related to thermo-hydrodynamic activities of the companion. This can be seen as follows. The thermodynamic adjustment of a star in response to external perturbation is constrained by the Kevin–Helmholtz timescale, which may be expressed in terms of the stellar mass M, stellar radius R, and stellar luminosity:

$$\tau_{\rm kh} = \frac{GM^2\xi}{2RL} \approx 3.1 \times 10^7 \, {\rm yr} \left(\frac{M}{\rm M_\odot}\right) \left(\frac{R}{\rm R_\odot}\right)^{-1} \left(\frac{L}{\rm L_\odot}\right)^{-1} \xi \,, \quad (4)$$

where G is the gravitational constant. Here, we introduce a variable $\xi = \Delta M/M$, where ΔM is mass of the layer at the stellar surface participating in the thermo-hydrodynamic response. Setting $\xi = 1$ will recover the standard expression for the Kevin–Helmholtz timescale of star, which is commonly used for stellar response to mass-loss (see e.g. Plavec, Ulrich & Polidan 1973). For low-mass stars with $(M/{\rm M_\odot}) \sim (0.2\text{–}0.4)$, $(M/{\rm M_\odot}) \sim (R/{\rm R_\odot})$ (see e.g. Demory et al. 2009). Also, $(L/{\rm L_\odot}) \sim (M/{\rm M_\odot})^4$ (see e.g. Wang & Zhong 2018). This gives $\tau_{\rm kh} \sim 3 \times 10^7 {\rm yr} \, (M/{\rm M_\odot})^{-4} \, \xi \gg 1 \, {\rm yr}$ for $(M/{\rm M_\odot}) \sim 0.2$, even when assuming an extremely small mass layer with $\xi \sim 10^{-7}$ (cf. Kovetz, Prialnik & Shara 1988; Sarna 1990; Ginzburg & Quataert 2021). Thus, the thermo-hydrodynamic response of the companion is unlikely to be the cause of the short-lived low states observed in Polars.

The magnetic activity of the system is, however, a viable alternative. It involves changes in the magnetic field configuration of the binary, which in turn disrupts the mass transfer process. This can be achieved, for instance, when a star-spot on the companion's surface migrates to a region near the L1 point (see Livio & Pringle 1994). Rotating convective stars are magnetically active, and star spots are expected to be present in the companion stars in CVs, including both Polars and IPs. In Polars, the magnetic field of the WD can also play a role as it is strong enough to influence the magnetic field configurations of the entire system. The magnetic field near the L1 point is not always dominated by the local magnetic field of the companion star, as the magnetic field of the WD and that of the companion star may be interconnected. As such, the mass transfer process is also associated with the interaction of the magnetic fields of the immigrated star-spot and of the WD at the L1 point (see e.g. Wu & Kiss 2008, for the influence of the WD magnetic fields on the mass transfer). While this coordinated magnetic interaction would lead to the short low states by the suppression of the mass transfer, it can also lead to brief mass transfer episodes fuelled by (active) magnetic channelling, which manifests as the short high stated seen in some Polars. The short-lived low states and the short-lived high states are therefore facets of the magnetic-interaction-regulated mass transfer dynamics, and we shall discuss this more thoroughly in the next

subsection, in the context of mass transfer models, (e.g. Lubow & Shu [1975](); Meyer & Meyer-Hofmeister [1983](); Osaki [1985](); Ritter [1988]()).

3.2 Short-lived high states

Short-lived high states are by far the least common feature which we have identified in this work – having identified only three systems. Despite this they show clear evidence of being repeated features with AP CrB showing evidence for as many as five events over ∼1400 d. These events are a result of a temporary increase in the rate of mass transfer within the system.

Much of the population of CVs, as IPs or Dwarf Novae, are known to be capable outbursts, even if individual systems have not been observed to do so. These outbursts are relatively short-duration (tens of days) events whereby accretion, by virtue of an instability, suddenly and temporarily increases. These outbursts are characterized broadly via their asymmetric temporal evolution – a sudden increase in brightness over a day or less, followed by a short plateau phase, and finally a gradual reduction in brightness (see Coppejans et al. [2016](), for a fuller discussion of CV outbursts).

Conversely, Polars are not known to be systems capable of dwarf nova outburst, because they lack the necessary accretion disc. Similarly the short-duration high states, which we report in this work, do not have the same temporal profile as outbursts seen in other systems – they are more symmetric in shape, resembling transitions in and out of previously observed long-duration states. As such, we are not proposing that these events are outbursts in Polars, but the very short duration does suggest that these state changes are unstable.

Accepting this, and further that the short-duration low states are related to star spots, we can explain the occurrence of the short-lived high states in a self-consistent manner, i.e. within the same framework of the coronal/atmospheric magnetic activities of the companion star. Doing so requires that we address several issues.

First, we must consider whether or not these high states are consequences of thermo-hydrodynamics activities. As discussed previously, this will require a timescale comparable to the Kevin–Helmholtz timescale. Applying the same argument as before, it is unlikely that thermo-hydrodynamics drives the system into such short episodes of high state.

Next, we need to look at whether or not there are sharp changes in the physical condition near the L1 point, where the mass transfer initiates. There are certain conditions that need to be satisfied for mass transfer to occur when the companion star is reaching the critical Roche surface of the binary, one of which is that the outflow must become transonic when the material crosses the L1 point. This gives a simple approximate expression for the mass transfer rate:

$$\dot{M} \sim [\rho \, c_{\mathrm{s}}(T)]_{\mathrm{L1}} \, \mathcal{A} \tag{5}$$

(see e.g. Lubow & Shu [1975](); Meyer & Meyer-Hofmeister [1983]()), where the mass density ρ, the isothermal sound speed c_{s}, and the stellar surface temperature T are evaluated at the L1 point at the critical Roche surface and $\mathcal{A}$ is the initial cross-section of the mass-outflow stream. As a first approximation, the atmospheric mass density at the L1 point would take the form

$$\rho \approx \rho_0 \, \exp\left[-\frac{1}{2}\left(\frac{\Delta r}{z_0}\right)^{\alpha}\right] , \tag{6}$$

where ρ_0 is density at the 'base' of the stellar atmosphere,[3] Δr is the separation length between the critical Roche surface and the surface of the 'base' of the stellar atmosphere, and z_0 can be considered as a reference scale height of the stellar atmosphere.[4] The index α may take a value between 2 for semidetached binaries, with consideration of the forces associated with binary rotation and atmospheric hydrodynamic in the companion star (Lubow & Shu [1975](); Meyer & Meyer-Hofmeister [1983](); Kovetz et al. [1988]()), and 1, for a hydrostatic atmosphere (Osaki [1985](); Ritter [1988]()).

In the presence of a magnetic field, the stellar material flowing from the secondary star will be subject to both gravitational and electromagnetic forces. Thus, the criterion in terms of solely the Roche potential is insufficient, as one needs to account for the electromagnetic force. We may decompose the force density exerted on the stellar material of density ρ near L1 point as

$$\boldsymbol{f} = \boldsymbol{f}_{\mathrm{g}} + \boldsymbol{f}_{\mathrm{B}} = -\rho \, \nabla \phi_{\mathrm{g}} + \boldsymbol{f}_{\mathrm{B}} , \tag{7}$$

with the subscripts 'g' and 'B' denoting gravitational origin and electromagnetic origin, respectively, and ϕ_{g} is the effective gravitational potential. The magnetic force density acting on the (partially) ionized material is given by

$$\boldsymbol{f}_{\mathrm{B}} = \frac{1}{4\pi}\left[(\boldsymbol{B} \cdot \nabla)\,\boldsymbol{B} - \frac{1}{2}\,\nabla\,B^2\right] , \tag{8}$$

where the first and second terms in the bracket correspond to the magnetic tensor force and the magnetic pressure gradient force, respectively. The strength of these forces on the stellar material depends on the degree of ionization of the stellar material near the L1 point, in addition to the magnetic-field strength and orientation. It is important to note that these magnetic forces are local quantities near the L1 point, contributed mostly by the presence of an migrating star-spot which interacts with the WD magnetic field. This is in contrast to ϕ_{g}, which is a global quantity of the binary defined by the gravitational field of the WD and the companion star and their orbital motion.

The presence of a local ϕ_{B} implies that the mass transfer rate is no longer regulated solely by the gravitational force within the binary and the thermo-hydrodynamic condition of the companion. Variations in ϕ_{B} near the L1 point would lead to variations in $\dot{M}$ regardless of other conditions in the companion star. We have attributed the low states as the disruption of ongoing mass transfer by an in-migration of a star-spot, such that a magnetic force temporally suppresses the outflow of material through the L1 point. In the same token, we may consider that the occurrence of the short high states corresponds to a temporary enhancement of mass flow across the gravitational surface through the magnetic channels. Such an enhancement may arise via interconnecting the WD magnetic field, when the companion star is very close to, but has not yet reached, the critical state that mass transfer proceeds in a natural manner (cf. Bonnet-Bidaud et al. [2000]()).

Flow suppression and enhanced magnetic channelling are caused by the migration of the star-spot to regions close to the L1 point, and so they would operate on similar timescales, at least in the

---

[3]The star is not spherical and the atmospheric base is ill defined. However, a reference location for the purpose of this work may be defined in terms of the optical depth, and following Kovetz et al. ([1988]()), we may take it as the location in the photosphere with optical depth, τ, at 2/3.

[4]Usually, for an isothermal stellar atmosphere, the atmospheric scale is given by $z_0 \sim k_{\mathrm{B}} T / \mu m_{\mathrm{H}} g$, where k_{B} is the Boltzmann constant, m_{H} is the hydrogen mass, μ is the mean molecular weight, T is the atmospheric temperature, and g is the surface gravity.

first-order approximation. Moreover, the high and low state light curves should share some inverted up-down similarity, which we see in the light curves presented here. This extension of the magnetic interaction mechanism such as that outlined in Wu & Kiss (2008) to incorporate the in-migration of star spots could explain the presence of short low states and short high states, and the existence of both short low states and short high states of the same system at different observational episodes, though we have seen no evidence of such systems. It overcomes some difficulties in the earlier versions of the star-spot model, e.g. the requirement that the high state is the default mass transfer state (see Livio & Pringle 1994) and explains short high and low states being more frequently found in Polars rather than in other CVs.

We now remark on why the magnetic field could still confine material outflow from the donor stars in Polars, which are generally low-mass M stars, with optical/IR photospheric emission with spectral temperatures of 2000–3000 K. We expect that gas at 2000–3000 K is not ionized and thus a neutral gas would not be magnetically confined when the Lorentz force is absent. Magnetic confinement can occur due to several very specific conditions in these systems. First of all, these low-mass M stars have magnetic coronal activities which produce high-energy charged particles. These charged particles are confined by the magnetic field and the neutral material is confined through the collision with the confined charged particles; the neutral material can only cross the magnetic field through ambipolar diffusion (see e.g. Spitzer 1978). This together with the transonic condition for material outflow from the L1 point (see Lubow & Shu 1975) gives the confinement condition $\chi n_p > 10^3$ cm^{-3}, where χ is the ionization fraction and n_p is the number density of particles at the L1 point (see the derivation in Appendix A). Provided that a non-negligible amount of ions are present and the material near the L1 point is sufficiently dense (so to maintain strong collision between particles), the magnetic field will have strong effect outflow of cool neutral gas.

3.3 Mass transfer rate during the transition between high and low states

The magnetic scenario linking the migration of star-spot(s) to the L1 point and the interaction between the magnetic fields of the star-spot and the WD seem to provide an adequate explanation of both the short-lived low states and the short-lived high states, even though the mechanisms likely differ in detail.

The successive occurrence of these states implies that clusters of star spots, instead of a giant isolated star-spot, is likely responsible. A remaining issue is what observational signature(s) would we expect for the mass transfer rate if these short state transitions are caused by magnetic activities near the L1 point when a high state transitions to a low state or vice versa. This magnetic interaction scenario does not require substantial changes in the global thermal structure of the companion star, and hence the variations and the stability in mass transfer are not driven by the variations in thermodynamics variables of the outer layer of the companion star. Instead, they are regulated by the magnetic field configurations, which are determined by the migrations of the star-spot, and the relative strength and orientation of the magnetic fields of the star spots and of the WD.

The magnetic field configuration at the L1 point can also be adjusted through processes, such as MHD interactions between the ionized material and the magnetic field at the L1 point and also events such as magnetic reconnections, which are eruptive in nature. As such, we would expect that the mass transfer rate would not change smoothly, when a Polar switches from a low state to a high state or

from a high state to a low state. Flare-like activities are expected if magnetic reconnections occur, as the mass outflow will be broken up into magnetized fluid chunks (see for instance the flare on the Polar MQ Dra Ramsay, Hakala & Wood 2021). This is also in contrast to the abrupt yet smooth change in the source brightness when it is caused by occultation (cf. e.g. the eclipse in the photometric light curves of CTCV J192−5001 Potter, Augusteijn & Tappert 2005).

3.4 Orbital folded light curves and mass transfer rate

The *TESS* data have allowed us to search for differences in the profile of the optical orbital light curves as a function of mass transfer rate (i.e. high/low states). In turn, this allowed us to address whether the stream couples on to different field lines depending on the accretion rate and therefore its ram pressure. At high mass transfer rates the ram pressure is high and can penetrate deeper into the WD magnetic field. This allows for material to reach field lines orginating from a second pole on the WD which under a lower mass transfer rate, and consequently ram pressure, they might not. The alternative model of 'blobby' accretion was proposed by Kuijpers & Pringle (1982) whereby individual 'blobs' of material penetrate the WD photosphere; this model has been used to explain the apparent difference in behaviour seen from the different poles (Hameury & King 1988; Schwope et al. 2020) and the soft X-ray excess seen in many Polars (Frank, King & Lasota 1988).

A further possible origin for the change of accretion geometry is asynchronous rotation whereby the WD has a (temporarily) marginally different spin period from the orbit of the system. The material latches on to different field lines as a result of the differential rotation, meaning the material can penetrate to different depths depending on the field lines in use. This change however is not associated with a change in mass transfer rate and thus is unlikely to apply in any of the systems presented in this work.

In each of those systems in this study where we see a low state, we also observe an associated change in the shape of the light curve, the nature of which seems somewhat variable, e.g. the first low state seen in CW Hyi shows a cessation of accretion, whereas the second shows it to continue in a similar way to as before the state but at a much suppressed rate. In AM Her and QQ Vul, we see the increased pronouncement of a second peak in the profile which has been observed before and are considered to be the revealing of features present during the high state but otherwise dominated by the primary accretion stream. In each of these cases, where accretion continues in the low state, the original light curve is still recognizable within the low state. It is either supplemented by an additional feature or continued at a lower flux rate. This suggests that no significant change in accretion geometry occurs in these low states, beyond the rate of accretion falling substantially.

MT Dra is the markedly different system out of the four systems with short-duration low states shown here; the orbital light curve of the low state follows a similar but suppressed profile of the brighter state following it, whereas the bright state proceeding it shows a different profile, albeit one which is related, with the same initial dip. We note that MT Dra is the only one of the four systems which has a period below the period gap. In contrast to those other systems MT Dra does appear to show a changing accretion geometry between the states.

V834 Cen was the only system which showed a short-lived high state which we were able to construct an orbital light curve. In this case, although the increased brightness implied an increased accretion rate, we show no evidence of a changed accretion geometry. It is therefore likely the case that the change ram pressure in the high

state is either insufficient to push deeper into the WD magnetic field or that in the initial state the accretion flow already penetrates to such a depth that any increase in the ram pressure is negligible relative to the magnetic energy density at that depth.

4 CONCLUSIONS

We have presented observations from *ZTF* and *TESS* of short-duration state changes as seen in a number of Polars. These observations reveal that short-duration state changes are a common feature in Polars. The observations from *TESS* in particular have revealed a number of especially short-duration state changes which without the coverage and cadence provided by *TESS* would have been hitherto hidden from us. The observations from *TESS* have allowed us to probe the accretion geometry of these systems by studying the changes in the orbital light curves during the various accretion states revealing how the material in-fall is altered in these different scenarios. The *TESS* observations also have allowed us to refine the orbital period of CW Hyi where we found a period of 181.55 min.

Considering these state changes has allowed us to generalize the scenario of star-spot migration traditionally adopted for explaining the occurrence of the low states to incorporate the interaction between the magnetic fields of the star spots and that of the WD. As such, we have developed a satisfactory explanation for both the short-duration low and high states within a self-consistent and unified framework, whereby the mass transfer rate is consequentially determined by the thermal and MHD conditions of the companion star at the L1 point, in the presence of the magnetic interaction between the star spots and the WD.

In order to advance this work into these different state changes further useful data to gain would include polarimetry and X-ray observations as this would allow for mapping of the accretion regions and understanding the mass transfer rates. In addition to this, further inclusion of Polars in upcoming *TESS* sectors would be useful to build up a more complete understanding of the number of systems which exhibit this behaviour, in particularly the shortest duration states, the frequency of this behaviour, and its breadth across the population of Polars.

DATA AVAILABILITY

TESS data are available from the Mikulski Archive for Space Telescopes (MAST), which can be accessed at https://mast.stsci.edu/portal/Mashup/Clients/Mast/Portal.html.

ZTF data are available via the NASA/IPAC Infrared Science Archive https://irsa.ipac.caltech.edu/Missions/ztf.html

REFERENCES

Agrawal P. C., Riegler G. R., Rao A. R., 1983, Nature, 301, 318
Belle K. E., Howell S. B., Mills A., 2000, PASP, 112, 343
Bellm E. C. et al., 2019, PASP, 131, 018002
Beuermann K., Euchner F., Reinsch K., Jordan S., Gänsicke B. T., 2007, A&A, 463, 647
Bonnet-Bidaud J. M. et al., 2000, A&A, 354, 1003
Brainerd J. J., Lamb D. Q., 1985, in Lamb D. Q., Patterson J., eds, Cataclysmic Variables and Low-Mass X-Ray Binaries. Springer, Dordrecht, p. 247
Burwitz V., Reinsch K., Beuermann K., Thomas H. C., 1997, A&A, 327, 183
Cieslinski D., Rodrigues C. V., Silva K. M. G., Diaz M. P., 2010, Inf. Bull. Var. Stars, 5957, 1
Coppejans D. L., Körding E. G., Knigge C., Pretorius M. L., Woudt P. A., Groot P. J., Van Eck C. L., Drake A. J., 2016, MNRAS, 456, 4441
Covington A. E. et al., 2022, ApJ, 928, 164
Cropper M., 1990, Space Sci. Rev., 54, 195
Cropper M., 1998, MNRAS, 295, 353
Cropper M., Menzies J. W., Tapia S., 1986, MNRAS, 218, 201
Demory B. O. et al., 2009, A&A, 505, 205
Ferrario L., Wickramasinghe D. T., Bailey J., Tuohy I. R., Hough J. H., 1989, ApJ, 337, 832
Foreman-Mackey D., Hogg D. W., Lang D., Goodman J., 2013, PASP, 125, 306
Frank J., King A. R., Lasota J. P., 1988, A&A, 193, 113
Gänsicke B. T., Fischer A., Silvotti R., de Martino D., 2001, A&A, 372, 557
Giampapa M. S., Rosner R., Kashyap V., Fleming T. A., Schmitt J. H. M. M., Bookbinder J. A., 1996, ApJ, 463, 707
Ginzburg S., Quataert E., 2021, MNRAS, 507, 475
Hakala P., Ramsay G., Potter S. B., Beardmore A., Buckley D. A. H., Wynn G., 2019, MNRAS, 486, 2549
Hameury J. M., King A. R., 1988, MNRAS, 235, 433
Hameury J. M., Lasota J. P., 2002, A&A, 394, 231
Hartquist T. W., Williams D. A., 1989, MNRAS, 241, 417
Hessman F. V., Gänsicke B. T., Mattei J. A., 2000, A&A, 361, 952
Hill K. L. et al., 2022, AJ, 163, 246
Honeycutt R. K., Kafka S., 2004, AJ, 128, 1279
Kafka S., Honeycutt R. K., 2003, AJ, 125, 2188
Kafka S., Honeycutt R. K., 2005, AJ, 130, 742
Kafka S., Honeycutt R. K., Howell S. B., Harrison T. E., 2005, AJ, 130, 2852
Kirby K. P., 1995, Phys. Scr. T, 59, 59
Kovetz A., Prialnik D., Shara M. M., 1988, ApJ, 325, 828
Kuijpers J., Pringle J. E., 1982, A&A, 114, L4
Leach R., Hessman F. V., King A. R., Stehle R., Mattei J., 1999, MNRAS, 305, 225
Lightkurve Collaboration, 2018, Astrophysics Source Code Library, record-dascl:1812.013
Livio M., Pringle J. E., 1994, ApJ, 427, 956

Lubow S. H., Shu F. H., 1975, ApJ, 198, 383

Mason P. A., Santana J. B., 2015, Proc. Sci., Low States of Polars: Catalina (CRTS) Light Curves. SISSA, Trieste, PoS(Golden2015)016

Mason K. O., Middleditch J., Cordova F. A., Jensen K. A., Reichert G., Murdin P. G., Clark D., Bowyer S., 1983, ApJ, 264, 575

Meyer F., Meyer-Hofmeister E., 1983, A&A, 121, 29

Middleditch J., Imamura J. N., Wolff M. T., Steiman-Cameron T. Y., 1991, ApJ, 382, 315

Mouchet M. et al., 2017, A&A, 600, A53

Newville M. et al., 2021, lmfit/lmfit-py: 1.0.3. https://doi.org/10.5281/zenodo.5570790

Nousek J. A. et al., 1984, ApJ, 277, 682

Olivero J., 1977, J. Quant. Spectrosc. Radiat. Transfer, 17, 233

Osaki Y., 1985, A&A, 144, 369

Plavec M., Ulrich R. K., Polidan R. S., 1973, PASP, 85, 769

Potter S. B., Augusteijn T., Tappert C., 2005, MNRAS, 364, 565

Ramsay G., Cropper M., Mason K. O., 1995, MNRAS, 276, 1382

Ramsay G., Hakala P., Wood M. A., 2021, MNRAS, 504, 4072

Ricker G. R. et al., 2015, J. Astron. Telesc. Instrum. Syst., 1, 014003

Ritter H., 1988, A&A, 202, 93

Romero-Colmenero E., Potter S. B., Buckley D. A. H., Barrett P. E., Vrielmann S., 2003, MNRAS, 339, 685

Sarna M. J., 1990, A&A, 239, 163

Schwarz R., Greiner J., Tovmassian G. H., Zharikov S. V., Wenzel W., 2002, A&A, 392, 505

Schwope A. D., Beuermann K., Thomas H. C., 1990, A&A, 230, 120

Schwope A. D., Thomas H. C., Beuermann K., Naundorf C. E., 1991, A&A, 244, 373

Schwope A. D., Thomas H. C., Beuermann K., Reinsch K., 1993, A&A, 267, 103

Schwope A. D., Catalán M. S., Beuermann K., Metzner A., Smith R. C., Steeghs D., 2000, MNRAS, 313, 533

Schwope A. D., Brunner H., Buckley D., Greiner J., Heyden K. v. d., Neizvestny S., Potter S., Schwarz R., 2002, A&A, 396, 895

Schwope A. D., Worpel H., Traulsen I., Sablowski D., 2020, A&A, 642, A134

Šimon V., 2016, MNRAS, 463, 1342

Spitzer L., 1978, Physical Processes in the Interstellar Medium. John Wiley & Sons, Ltd., Hoboken, NJ

Szkody P. et al., 2002, AJ, 123, 430

Tapia S., 1977, ApJ, 212, L125

Wang J., Zhong Z., 2018, A&A, 619, L1

Warner B., 1995, Cataclysmic Variable Stars, Cambridge Astrophysics. Cambridge Univ. Press, Cambridge

Wickramasinghe D. T., Wu K., 1991, MNRAS, 253, 11P

Wickramasinghe D. T., Ferrario L., Bailey J., 1989, ApJ, 342, L35

Wickramasinghe D. T., Bailey J., Meggitt S. M. A., Ferrario L., Hough J., Tuohy I. R., 1991, MNRAS, 251, 28

Wu K., 2000, Space Sci. Rev., 93, 611

Wu K., Kiss L. L., 2008, A&A, 481, 433

Wu K., Wickramasinghe D. T., 1993, MNRAS, 260, 141

Wu K., Wickramasinghe D. T., Warner B., 1995, Publ. Astron. Soc. Aust., 12, 60

Zubareva A. M., Pavlenko E. P., Andreev M. V., Antipin S. V., Samus' N. N., Sergeev A. V., 2011, Astron. Rep., 55, 224

APPENDIX A: MAGNETIC CONFINEMENT OF OUTFLOW OF COOL MATERIAL AT THE L1 POINT

The donor stars in Polars are mostly low-mass M stars. Although they are considered cool in terms of the spectral temperature of their photospheric emission, they are magnetically active and have a corona. The gas in their corona is ionized and it is also collisional in nature (Giampapa et al. 1996). The interaction of the magnetized plasma in the corona results in the ionized gas mixing with the cooler gas at the stellar surface, which gives rise to the optical/IR photospheric emission of the star. While the charged particles are strongly coupled with the magnetic field, neutral gas with temperature as low as 2000–3000 K, indicated by the photospheric emission from M star, would, in principle, not be confined magnetically. However, because of collisions between the neutral atoms and the charged particles, their mobility would be restricted by the magnetic field. The neutral gas therefore does not free stream across the magnetic field but undergoes an ambipolar diffusion, which may be described by the following relation:

$$\alpha_{in} n_i \rho v_d \approx \frac{B^2}{4\pi L} \tag{A1}$$

(see Spitzer 1978), where n_i is the number density of ions, ρ is the mass density of the medium, v_d is the diffusion speed, and L is the characteristic linear size of the medium where the neutral gas diffuses across. The collisional rate between the neutral and charged particles, α_{in}, in astrophysical systems generally have values about 10^{-9} cm^3 s^{-1} (see Hartquist & Williams 1989; Kirby 1995).

We may express the number density of ions in terms of the total number density of atomic particles as $n_i = \chi n_p$, with χ as a parameter effectively indicating the ionization faction. Magnetic confinement requires that

$$\frac{B^2}{8\pi \rho c_s^2} > 1 \,, \tag{A2}$$

where c_s is the local isothermal sound speed of the particles confined by the magnetic field. It follows that the criterion for magnetic confinement of ions and particles in the presence of ambipolar diffusion is given by

$$\frac{\alpha_{in} \chi n_p v_d L}{2 c_{s,n}^2 \left[(1-\chi) + \chi (c_{s,i}/c_{s,n})^2 \right]} > 1 \,, \tag{A3}$$

where $c_{s,n}$ and $c_{s,i}$ are the thermal sound speeds of the neutral particles and the ions, respectively.

For mass transfer in low-mass semidetached binaries, the outflow from the donor stars at the L1 point is transonic (see Lubow & Shu 1975). With this condition, we have $\text{Max}(v_d) \sim |c_{s,n} - c_{s,i}| \approx c_{s,i}$, and the confinement condition becomes

$$\chi n_p > \frac{2 c_{s,n}^2}{\alpha_{in} L c_{s,i}} \,. \tag{A4}$$

Assuming $L \sim 10^9$ cm, $c_{s,n} \approx 10^5$ cm s^{-1} (corresponding to a thermal temperature of 2000 K) and $c_{s,i} \approx 2 \times 10^7$ cm s^{-1} (corresponding to a thermal temperature of 10^6 K) gives

$$\chi n_p > 10^3 \text{cm}^{-3} \,. \tag{A5}$$

Thus, the presence of a small amount of ions would be able to hold the neutral gas at the L1 point. To violate the confinement condition, it requires a very low matter density and a low ionization such that $\chi n_p < 10^3$ cm^{-3}, or the presence of a strong external force that has, however, built up to counterbalance the magnetic stress force. Alternatively, the condition does not hold if the transonic condition for mass transfer in low-mass semidetached systems as that derived by Lubow & Shu (1975) is invalid.

APPENDIX B: COMPLETE LIST OF ZTF SOURCES

Table B1. ZTF sources considered. A number of sources show no values, which is because they were excluded from analysis as they had fewer than 25 data points in both filters. The state changes column relates to the presence of short duration, long-duration state changes, both, or none.

Source	g mean	g min	g max	r mean	r min	r max	No. data points	State changes
2XMM J183251.4−100106	17.8	17.94	17.58	17.47	20.5	15.57	1569	None
2XMMp J1313223.4+173659	19.09	20.48	18.01	19.03	20.41	17.92	2179	None
AM Her	14.26	15.47	12.79	13.99	15.33	12.28	1843	Both
AN UMa	17.21	19.17	15.88	17.09	18.86	15.85	843	Short
AP CrB	17.4	17.73	16.14	17.42	17.78	16.2	543	Short
AR UMa	16.36	16.41	16.31	16.59	16.7	16.51	118	None
BS Tri	18.2	20.5	17.03	17.84	20.24	16.64	924	Short
BY Cam	15.38	16.2	14.4	14.97	16.07	13.71	726	None
CSS0357+10	19.34	20.39	18.09	18.49	19.46	17.3	91	None
CSS2335+12	19.17	20.47	17.66	18.83	20.18	17.59	579	None
DDE23	19.19	19.97	17.99	18.77	19.89	17.42	3808	None
DP Leo	18.76	19.99	18.19	18.62	20.2	18.03	267	None
EF Eri	18.13	18.3	17.97	18.28	18.41	18.16	145	None
EG Lyn	18.62	19.09	18.01	18.39	18.87	17.76	83	None
EK UMa	18.96	20.43	17.74	18.94	20.18	17.88	948	None
EP Dra	18.35	20.43	17.29	18.23	20.43	16.84	1548	None
EQ Cet	18.02	19.0	16.79	17.94	18.96	16.85	227	None
EU Cnc	–	–	–	–	–	–	10	–
EU UMa	18.4	19.32	17.04	18.39	20.5	16.72	1512	Short
EV UMa	17.67	20.5	15.89	17.85	20.47	16.23	1246	Long
FH UMa	–	–	–	–	–	–	38	–
FL Cet	19.15	20.12	17.01	19.01	19.96	16.37	437	Short
GG Leo	18.19	19.34	16.39	17.87	19.25	16.12	374	None
HS Cam	19.98	20.5	18.14	19.86	20.5	17.83	798	Short
HU Aqr	16.24	18.65	14.63	17.09	20.49	14.58	412	None
HY Eri	19.59	20.5	18.79	19.41	20.49	18.4	1072	None
IW Eri	18.68	19.87	16.28	18.65	19.92	16.27	264	Long
LW Cam	18.01	20.49	15.43	18.63	20.5	15.22	760	Long
MN Hya	18.02	19.79	16.58	18.08	19.72	16.72	51	None
MQ Dra	18.69	19.14	18.24	17.49	18.13	16.93	1689	None
MR Ser	–	–	–	–	–	–	27	–
MT Dra	18.12	20.49	17.01	17.6	20.48	16.44	1959	Short
PBC J0706.7+0327	17.14	17.66	16.61	17.11	17.73	16.39	1154	None
QQ Vul	15.05	17.05	14.37	14.87	16.37	14.16	1109	None
RX J0325−08	17.59	18.54	15.48	17.2	18.48	15.01	418	None
RX J0502.8+1624	19.05	19.32	18.44	19.0	19.29	17.78	545	None
RX J0524+4244	17.35	18.05	16.41	17.36	18.13	16.39	818	None
RX J0600−2709	19.72	20.2	19.2	19.59	20.41	18.9	598	None
RX J0649−0737	17.24	18.83	16.24	16.75	17.9	16.25	398	None
RX J0749-0549	18.73	20.37	17.31	19.4	20.3	16.98	659	Long
RX J0953+1458	18.86	20.45	16.56	18.33	20.43	16.42	408	None
RX J1002−19	18.43	19.63	17.07	18.81	20.32	17.22	176	None
RX J1007−20	18.5	20.29	16.77	18.15	19.54	16.53	183	None
RX J1610+03	17.49	19.07	16.24	16.98	18.65	15.33	403	Short
RX J2015.6+3711	18.69	19.07	16.54	17.51	17.87	15.85	1258	None
RX J2316−05	19.55	20.2	17.85	18.98	19.8	16.91	326	None
SDSS J032855+052254	19.36	20.45	17.5	19.13	20.49	17.48	317	None
SDSS J072910+365838	20.14	20.49	19.19	19.91	20.49	18.87	779	None
SDSS J075240+362823	16.91	16.97	16.78	16.34	16.4	16.29	816	None
SDSS J085414+390537	18.59	19.93	15.61	18.61	20.31	15.88	772	None
SDSS J085909+053654	18.48	19.21	17.67	18.15	19.0	16.5	654	None
SDSS J092122+2038571	–	–	–	–	–	–	124	–
SDSS J103100+202832	18.12	20.48	16.44	18.26	20.14	16.79	380	Long
SDSS J121209+013627	17.96	18.07	17.82	18.09	18.21	17.97	497	None
SDSS J1333092+1437069	20.01	20.49	19.39	19.78	20.46	18.52	71	None
SDSS J142256−022108	19.4	20.45	18.56	19.23	20.32	18.38	276	None
SDSS J154104+360252	18.03	20.2	15.99	17.76	20.2	15.52	1466	Long
SDSS J170053+4000357	18.84	20.46	16.49	18.47	20.48	16.34	1743	None
SDSS J204827+005008	19.48	19.95	18.53	18.74	19.13	18.22	355	None
ST LMi	16.61	17.66	15.15	16.31	17.63	14.38	507	Short
Swift J2341.0+7645	18.35	20.0	16.96	17.59	19.04	16.3	658	Long

Table B1 – *continued*

Source	g mean	g min	g max	r mean	r min	r max	No. data points	State changes
UZ For	16.95	20.43	15.77	17.0	20.3	15.84	217	None
V1007 Her	–	–	–	–	–	–	2	–
V1309 Ori	16.21	18.07	15.08	15.83	20.49	15.04	883	None
V1432 Aql	15.91	20.05	14.78	15.89	19.0	14.53	619	None
V1500 Cyg	19.05	19.75	18.4	18.29	19.79	17.76	1778	None
V2301 Oph	17.22	20.32	16.12	17.38	20.03	15.91	1723	Short
V388 Peg	19.19	20.5	17.32	19.05	20.48	16.98	434	Both
V884 Her	15.98	16.8	14.41	15.8	16.99	14.28	1497	Short
VY For	18.01	19.66	16.6	17.78	19.45	16.58	184	Long
WX LMi	17.57	17.83	17.27	16.89	17.08	16.57	279	None

This paper has been typeset from a TEX/LATEX file prepared by the author.